

# Relativistic Navier-Stokes description of the quark-gluon plasma radial flow

Yago Bea

*Departament de Física Quàntica i Astrofísica and Institut de Ciències del Cosmos (ICC), Universitat de Barcelona, Martí i Franquès 1, ES-08028, Barcelona, Spain*

March 6, 2025

## Abstract

The relativistic viscous hydrodynamic description of the quark-gluon plasma by Müller-Israel-Stewart formulations has been very successful, but despite this success, these theories present limitations regarding well-posedness and causality. In recent years, a well-behaved version of the relativistic Navier-Stokes equations has been formulated, appearing as a promising alternative in which those limitations are absent. Using this novel theory, we perform numerical simulations of a quark-gluon plasma fluid that we use to describe experimental data on the transverse momentum distribution of hadrons from central Pb–Pb collisions measured at the LHC.

## Contents

<b>1</b>	<b>Introduction</b>	<b>2</b>
<b>2</b>	<b>The relativistic Navier-Stokes equations</b>	<b>4</b>
2.1	Frames: type I and type II . . . . .	5
2.2	Well-posedness and characteristic velocities . . . . .	6
<b>3</b>	<b>Numerical evolutions</b>	<b>7</b>
3.1	QCD equation of state and transport coefficients . . . . .	8
3.2	Initial data . . . . .	9
3.3	Numerical evolutions . . . . .	10
3.4	Description of the experimental data . . . . .	11
3.5	Effective field theory analysis . . . . .	13
<b>4</b>	<b>Discussion</b>	<b>16</b>
<b>A</b>	<b>Numerical code and convergence test</b>	<b>17</b>
<b>B</b>	<b>Well-posedness for a general stress tensor</b>	<b>18</b>

# 1 Introduction

Relativistic hydrodynamics is an effective theory useful for describing a microscopic underlying theory in a state of near local thermal equilibrium. From the perspective of effective field theory (EFT), relativistic hydrodynamics can be understood as a gradient expansion in which the zeroth order term is ideal hydrodynamics, with gradient corrections including dissipative effects. The system is considered to be in the EFT regime when gradient corrections are small. This situation is expected when there is a separation between the microscopic scale of the underlying theory and the macroscopic characteristic scale of the system. For a large separation of scales, gradient corrections are negligible, and ideal hydrodynamics offers a good approximation. If the separation of scales is not very large, viscous effects are expected to become relevant.

Relativistic hydrodynamics plays an important role in the description of the quark-gluon plasma (QGP) created in heavy-ion collision experiments at RHIC and LHC [1–5]. The resulting fireball is several times larger than the microscopic scale of quantum chromodynamics (QCD), suggesting that the system may approach a state of near local thermal equilibrium; this is confirmed by the fact that viscous hydrodynamics provides a good description of the experimental data. Further experimental efforts include the beam energy scan at RHIC [6] and upcoming experiments at FAIR or NICA. These experiments will be relevant to access the unexplored region of non-vanishing chemical potential in the QCD phase diagram. Moreover, having experimental access to transport properties may be useful to better discriminate between phases.

The relativistic version of the Navier-Stokes equations as originally written many decades ago by Eckart [7] and Landau and Lifshitz [8] was observed to present severe causality issues and instabilities [9]. Meanwhile, the experimental data of the QGP required a viscous hydrodynamic description [10]. In the absence of a well-behaved version of the relativistic Navier-Stokes equations, an approach that was useful to provide a relativistic viscous hydrodynamics description was a formulation introduced by Müller, Israel and Stewart (MIS) [11–13]. The idea of this approach is to consider the hydrodynamic expansion up to second order in gradients, and then promote the dissipative part of the stress tensor to be a new variable with its own evolution equation; the new set of equations exhibits better properties, alleviating the problems present in first-order viscous hydrodynamics. Based on this idea, different variants have been constructed, for example: BRSSS [14], DNMR [15], divergence-type theories [16–18], etc.; we collectively refer to them as ‘MIS theories’. The MIS approach became a standard tool for the experimental description of the QGP produced in heavy-ion collisions, and it is implemented in well-developed codes like MUSIC [19–21], SONIC [22] or VISHNU [23].

Despite this success, the MIS theories were found to present limitations. Although the MIS theories alleviate the problems present in the original version of the relativistic Navier-Stokes equations, allowing for a successful description of the experimental data, these problems are not completely solved. It was only in recent years that a proof of well-posedness was obtained for the first time for one specific version of these MIS theories [24]; for many years, the equations were used to describe experimental data without a proof of well-posedness, and for most of the formulations a proof is still lacking today. By checking these well-posedness and causality conditions in realistic numerical evolutions for the description of the QGP, significant violations were found [25–28], mainly at the initial stages of the evolution when gradients are larger. These violations might potentially affect the interpretation of the experimental data. Certainly, the experimental data has been successfully described to a large extent, so the consequences may not be very dramatic. But how specifically these limitations influence the analysis of the experimental data is still an open problem. Actually, if one wants to understand this influence, it is required a theory of viscous hydrodynamics that does not present these limitations, like the formulation that we now present.

For decades, the problem of why the relativistic version of the Navier-Stokes equations suffered from severe issues remained unsolved. That is, a theory that is meant to provide the effective description of any relativistic fluid near local thermal equilibrium, seemed to be unphysical. It was only in recent years that a solution was proposed: Bemfica, Disconzi, Noronha [29–31] and Kovtun [32] (BDNK) analyzed the well-posedness of the equations in a generic hydrodynamic frame, finding that in some specific frames the equations satisfy good properties of well-posedness and causality. In the language of EFT, a hydrodynamic frame corresponds to a perturbative field redefinition. The Eckart and Landau frames do not belong to this set of frames, explaining why, as originally written, the equations are not well-behaved.

We now may wonder a very natural question: if the MIS theories are successful describing the experimental data, why do we need another formulation of relativistic viscous hydrodynamics like relativistic Navier-Stokes? Is one theory ‘better’ in some sense than the other? We argue that relativistic Navier-Stokes has better properties of local well-posedness than MIS theories, which is an advantage at a fundamental level. In MIS theories the properties of well-posedness depend on the local energy density, and they must be checked pointwise in spacetime for every evolution, allowing for possible violations as the ones presented above. On the contrary, for relativistic Navier-Stokes a hydrodynamic frame can be chosen such that good properties of well-posedness are ensured at every point of spacetime for every evolution.

We now add a second argument, based on the principles of relativity. In MIS theories the characteristic speeds, that is, the ability of the equations to propagate information, also depend on the state and it could happen that in some regions of spacetime they exceed the speed of light. In relativistic Navier-Stokes a frame can be chosen such that the characteristic speeds are not faster than the speed of light, ensuring that the principles of relativity are satisfied.

Even at this point, we may still wonder: could one theory describe the experimental data ‘better’ than the other? In principle, we should not expect a hydrodynamics theory to describe better the experimental data than the other because both theories should provide equivalent descriptions if they are in the EFT regime, as it should be if we want them to provide a good description of QCD. We may claim that a theory is ‘better’ than the other at a fundamental level of well-posedness and causality, and this may have some impact in the description of the experimental data: if a theory present problems of well-posedness, it will not be useful for that description.

We now illustrate another example in which MIS theories have been shown to present limitations. There is increasing evidence that in neutron star mergers weak processes may play a relevant role in the postmerger dynamics, as they operate on similar timescales, giving rise to an effective bulk viscosity [33]. Evaluating the relevance of these viscous effects is an active area of research, and viscous neutron star mergers have been simulated using MIS formulations [34, 35], finding that in some regions of spacetime the well-posedness and causality conditions are violated.

As described above, mathematical properties of well-posedness and causality have been established for the relativistic Navier-Stokes equations, but one may wonder if these equations admit solutions. Numerical studies of real-time evolutions of the relativistic Navier-Stokes equations [36–40] provided evidence that they admit physically sensible solutions.

We go beyond the state of the art by performing real-time numerical evolutions of the relativistic Navier-Stokes equations with a QCD equation of state and transport parameters that we use to describe the QGP created in central heavy-ion collisions. For this purpose we consider a boost invariant, axially symmetric system to model the hydrodynamic radial flow expansion of the QGP, and we proceed to numerically solve the 1+1 Partial Differential Equations (PDEs). In our solutions we determine the freezeout surface at which we perform the conversion from the fluid to particles by using the Cooper-Frye prescription, obtaining a transverse momentum

distribution of hadrons that we use to describe experimental data of central Pb–Pb collisions at center of mass energy  $\sqrt{s_{NN}} = 2.76$  TeV measured by ALICE [41], finding good agreement.

This constitutes a first step of the implementation of the relativistic Navier-Stokes equations into the description of the QGP created in heavy-ion collision experiments. We consider a simple setup for the physics of the QGP like restricting to central collisions, simple geometrical initial data, or neglecting hadron physics after freezeout, because our main goal is to provide a proof of principle that the relativistic Navier-Stokes equations are useful for practical applications. For this purpose, we focus on the particularities of the Navier-Stokes equations: choosing appropriate frames, the initial data, the numerical implementation, etc.; once these particularities have been understood, extensions to more general scenarios can be considered. Also, one can obtain inspiration to proceed with extensions by following the infrastructure already available with the current MIS-based codes.

Moreover, we perform an EFT analysis of our solutions. This is motivated by the fact that only solutions to the hydrodynamics equations that are in the EFT regime are expected to provide a good description of QCD. Furthermore, we explore the effect of using different hydrodynamic frames to verify that the physics that is being described is independent on the arbitrarily chosen frame; otherwise the equations would lose predictive power.

The interested reader may jump to section 4 Discussion for a summary and conclusions.

## 2 The relativistic Navier-Stokes equations

We consider a fluid with equation of state

$$p(\epsilon), \quad (2.1)$$

Where  $\epsilon$  is energy density and  $p$  is pressure. The speed of sound  $c_s$  is given by

$$c_s^2 := \frac{\partial p(\epsilon)}{\partial \epsilon}, \quad (2.2)$$

The 4-velocity  $u^\mu$  is normalized such that  $u^\mu u_\mu = -1$ . We define the projector transverse to the velocity  $\Delta^{\mu\nu} := g^{\mu\nu} + u^\mu u^\nu$ , the comoving time derivative  $\dot{\epsilon} := u^\mu \nabla_\mu \epsilon$ , the comoving space derivative  $\nabla_\perp^\mu := \Delta^{\mu\nu} \nabla_\nu$ , the shear tensor  $\sigma^{\mu\nu} := \nabla_\perp^\mu u^\nu + \nabla_\perp^\nu u^\mu - 2/3 \Delta^{\mu\nu} \nabla_\alpha u^\alpha$  and vorticity  $\omega^{\mu\nu} := (\nabla_\perp^\mu u^\nu - \nabla_\perp^\nu u^\mu) / 2$ .

The constitutive relations of ideal hydrodynamics are

$$T^{\mu\nu} = \epsilon u^\mu u^\nu + p \Delta^{\mu\nu}, \quad (2.3)$$

The dynamical equations are given by the conservation of the stress-energy tensor

$$\nabla_\mu T^{\mu\nu} = 0, \quad (2.4)$$

Which explicitly are

$$\frac{\dot{\epsilon}}{\epsilon + p} + \nabla \cdot u = 0, \quad (2.5a)$$

$$\dot{u}^\mu + \frac{\partial p}{\partial \epsilon} \frac{\nabla_\perp^\mu \epsilon}{\epsilon + p} = 0, \quad (2.5b)$$

Where  $\nabla \cdot u := \nabla_\mu u^\mu$ . The constitutive relations up to first order in the gradient expansion of hydrodynamics for a non-conformal fluid in the Landau frame are [8]

$$T^{\mu\nu} = \epsilon u^\mu u^\nu + p \Delta^{\mu\nu} - \eta \sigma^{\mu\nu} - \zeta \nabla \cdot u \Delta^{\mu\nu}, \quad (2.6)$$

with  $\eta$  the shear viscosity and  $\zeta$  the bulk viscosity.

In the spirit of effective field theory, we consider a field redefinition of the fundamental fields  $\{\epsilon, u^\mu\}$  by first order terms in the hydrodynamics gradient expansion. The allowed terms by Poincare symmetry are the scalars  $\{\dot{\epsilon}, \nabla \cdot u\}$  and the vectors  $\{\dot{u}^\mu, \nabla_\perp^\mu \epsilon\}$ . We consider the following field redefinitions

$$\epsilon \rightarrow \epsilon + \mathcal{A}, \quad (2.7a)$$

$$u^\mu \rightarrow u^\mu + \frac{\mathcal{Q}^\mu}{\epsilon + p}, \quad (2.7b)$$

With

$$\mathcal{A} := a_1 \left( \eta + \frac{3}{4} \zeta \right) \left( \frac{\dot{\epsilon}}{\epsilon + p} + \nabla \cdot u \right), \quad (2.8a)$$

$$\mathcal{Q}^\mu := a_2 \left( \eta + \frac{3}{4} \zeta \right) \left( \dot{u}^\mu + \frac{\partial p}{\partial \epsilon} \frac{\nabla_\perp^\mu \epsilon}{\epsilon + p} \right). \quad (2.8b)$$

Where  $\{a_1, a_2\}$  are functions of the energy density that specify the field redefinition. An overall factor  $(\eta + 3/4\zeta)$  is introduced for convenience. The field redefinition (2.8) is not the most generic field redefinition compatible with Poincare symmetry, but it is a convenient subset interesting for practical applications, as we describe below.

Under a field redefinition (2.7) the stress tensor (2.6) becomes

$$T^{\mu\nu} = (\epsilon + \mathcal{A}) u^\mu u^\nu + (p + c_s^2 \mathcal{A}) \Delta^{\mu\nu} + \mathcal{Q}^\mu u^\nu + u^\mu \mathcal{Q}^\nu - \eta \sigma^{\mu\nu} - \zeta \nabla \cdot u \Delta^{\mu\nu}, \quad (2.9)$$

Where second and higher order terms in the gradient hydrodynamics expansion are neglected. The dynamical equations are derived by substituting (2.9) into the conservation equation (2.4)

$$\dot{\epsilon} + (\epsilon + p) \nabla \cdot u = -\dot{\mathcal{A}} - ((1 + c_s^2) \mathcal{A} - \zeta \nabla \cdot u) \nabla \cdot u - \nabla \cdot \mathcal{Q} + u \cdot \dot{\mathcal{Q}} + \frac{1}{2} \eta \sigma_{\mu\nu} \sigma^{\mu\nu}, \quad (2.10a)$$

$$\begin{aligned} (\epsilon + p) \dot{u}^\mu + c_s^2 \nabla_\perp^\mu \epsilon = & -((1 + c_s^2) \mathcal{A} - \zeta \nabla \cdot u) \dot{u}^\mu - \nabla_\perp^\mu (c_s^2 \mathcal{A} - \zeta \nabla \cdot u) + \Delta_\lambda^\mu \nabla_\nu (\eta \sigma^{\nu\lambda}) \\ & - \dot{\mathcal{Q}}^\mu - \frac{4}{3} \nabla \cdot u \mathcal{Q}^\mu - u \cdot \dot{\mathcal{Q}} u^\mu - \mathcal{Q}_\nu \left( \frac{1}{2} \sigma^{\nu\mu} + \omega^{\nu\mu} \right). \end{aligned} \quad (2.10b)$$

These are the *relativistic Navier-Stokes equations*, written in a general frame.<sup>1</sup> For each frame, a different set of PDEs is obtained, so there is not just ‘the relativistic Navier Stokes equations’ but a family of relativistic Navier-Stokes equations, one for each field redefinition, that is, for each pair of functions  $\{a_1, a_2\}$  [32]. The Landau frame corresponds to the particular case  $\{a_1, a_2\} = \{0, 0\}$ .

The fundamental reasons to consider the subset of frames (2.7) are

- They do not change the physical content to first order.
- They ‘regulate’ the Navier-Stokes equations so that they are well behaved.

We explain these statements in the following two subsections, respectively.

## 2.1 Frames: type I and type II

If one is familiar with the Landau frame but not with a more general frame, one may wonder what is the significance of the new terms  $\mathcal{A}, \mathcal{Q}^\mu$  in (2.9). Let us emphasize an important aspect:

<sup>1</sup>In this paper we use equivalently the nomenclature ‘relativistic first-order viscous hydrodynamics’, ‘relativistic Navier-Stokes’ or ‘BDNK’ to refer to the equations (2.10).

$\mathcal{A}$ ,  $\mathcal{Q}^\mu$  terms are proportional to the ideal equations of motion (2.5) and thus they are of second or higher order on-shell, that is, by using the equations of motion (2.10). Then, they do not modify the physical content of the equations up to first order in the hydrodynamic expansion, as long as the system is in the EFT regime. So, the interpretation of the physical quantities is as in the usual Landau frame:  $\epsilon$  is the energy density in the local rest frame of the fluid and  $u^\mu$  is the corresponding eigenvector, the local fluid velocity.

In the presence of chemical potential, that we do not consider in this paper, the traditional definitions of the Landau frame and Eckart frame correspond to different physical meanings of the fluid velocity: in the first case  $u^\mu$  corresponds to the velocity of the energy density and in the second case to the velocity of the charge density. This is in consonance with the fact that the field redefinition relating them is by first order terms which are not proportional to the ideal equations of motion. Thus, we find convenient to classify the field redefinitions into two categories:

- **Type I** Field redefinitions by terms not proportional to the ideal equations of motion.
- **Type II** Field redefinitions by terms proportional to the ideal equations of motion.

Type I field redefinitions introduce a difference in the physical meaning of the fundamental variables [32]. The field redefinition from the Eckart to the Landau frame is of type I. Notice that this still correspond to two different ways of parametrizing the same physics, in such a way that the prediction for the stress tensor should be equivalent to first order, just expressed in variables with different meanings. Type II field redefinitions, being proportional to the ideal equations of motion, are second or higher order on-shell, and thus they do not change the physical meaning of the fundamental variables up to first order. Our field redefinitions (2.7) are of type II.

For completeness, let us now consider the most general field redefinition for a non-charged fluid allowed by Poincare symmetry [32]

$$\epsilon \rightarrow \epsilon + \epsilon_1 \frac{\dot{\epsilon}}{\epsilon + p} + \epsilon_2 \nabla \cdot u , \quad (2.11a)$$

$$u^\mu \rightarrow u^\mu + \frac{\lambda}{\epsilon + p} \left( \dot{u}^\mu + \frac{\partial p}{\partial \epsilon} \frac{\nabla_\perp^\mu \epsilon}{\epsilon + p} \right) , \quad (2.11b)$$

Where  $\{\epsilon_{1,2}, \lambda\}$  are functions of the energy density that determine the field redefinition. Recall that in (2.11b) there is only one parameter  $\lambda$ , instead of two, due to extensivity [32]. Our field redefinitions (2.7) correspond to the subset obtained by imposing  $\epsilon_1 = \epsilon_2$  in (2.11), and redefining  $\epsilon_1 = a_1(\eta + 3/4\zeta)$ ,  $\lambda = a_2(\eta + 3/4\zeta)$ . We leave for future work the exploration of numerical evolutions in frames of type I in which  $\epsilon_1 \neq \epsilon_2$ , and we emphasize that considering frames of type II is sufficient and simpler for the purposes of describing the QGP. Conformal symmetry imposes  $\epsilon_1 = \epsilon_2$ , so in conformal fluids only type II frames are allowed [29, 32].

## 2.2 Well-posedness and characteristic velocities

We have argued that field redefinitions (2.7) do not modify the physical content of the relativistic Navier-Stokes equations; however, they modify the principal part of the equations, that is, the terms with highest derivatives, having an impact on the properties of well-posedness.

The first-order viscous hydrodynamics equations (2.10) have a locally well-posed initial value problem (Cauchy problem) and exhibit no faster than light propagation if

$$a_1 \geq \frac{4}{3c_s^2} , \quad a_2 \geq \frac{a_1}{\frac{3}{4}(1 - c_s^2)^2 a_1 - c_s^2} . \quad (2.12)$$

These expressions satisfy the more general expressions presented in [30,42], that are also provided in Appendix B. The simplicity of expressions (2.12) is another important reason to choose the specific subset of frames (2.7). In our numerical evolutions below we use frames satisfying (2.12).

We emphasize that the Landau frame  $\{a_1, a_2\} = \{0, 0\}$  does not belong to the subset of frames (2.12). This explains why the relativistic Navier-Stokes equations as originally written in Landau's book [8] are not well-behaved. In order to have a well-behaved version of the relativistic Navier-Stokes equations, necessarily both terms  $\mathcal{A}, \mathcal{Q}^\mu$  must be non-vanishing. In this sense, we can think of the terms  $\mathcal{A}, \mathcal{Q}^\mu$  as 'regulators', because keeping the physics to first order invariant, they allow to restore good properties of well-posedness.

Recall that the characteristic velocities of a PDE indicate the ability to propagate information. In order to satisfy the principles of relativity, the characteristic speeds must not exceed the speed of light, and this is satisfied by frames (2.12). The characteristic velocities  $\{c_{1,2,3,4}\}$  of the PDEs (2.10) are

$$c_i = \pm \sqrt{c_s^2 + 2 \frac{a_1 \pm \sqrt{a_1(a_1 + 3a_2(a_1 + a_2)c_s^2)}}{3a_1a_2}}. \quad (2.13)$$

We consider the following frame

$$\{a_1, a_2\} = \left\{ \frac{25}{12c_s^2}, \frac{100}{75 - 150c_s^2 + 27c_s^4} \right\}, \quad (2.14)$$

For which the characteristic velocities are

$$c_i = \pm 1, \pm \frac{3}{5}c_s^2. \quad (2.15)$$

Notice that finding a frame that satisfies the conditions (2.12) for every value of energy density is not obvious a priori, and (2.14) provides one such example. The fact that the conditions are satisfied for every value of the energy density ensures that it will be satisfied at every point of spacetime for every evolution, being this a major advantage over MIS theories. Frame (2.14) is also interesting because the largest characteristic velocity equals the speed of light, saturating the second inequality in (2.12), and thus it is expected to allow for the description of arbitrarily strong shockwaves [38,43]. Having constant characteristic speed and equal to the speed of light is another advantage over MIS; in the case of MIS theories the characteristics depend on the state, and if a solution explores velocities larger than the characteristics, the evolution might present problems, loosing predictive power.

### 3 Numerical evolutions

We consider our fluid in 3+1 dimensional Minkowski spacetime. We assume boost invariance along one spatial direction, that we identify with the beam axis, and axial symmetry in the transverse plane, with the purpose of modelling central collisions. We use adapted coordinates to this system: polar coordinates in the transverse plane and Milne coordinates along the beam axis direction,  $\{\tau, r, \phi, \eta_s\}$ , which are related to Cartesian coordinates  $\{t, x, y, z\}$  by

$$t = \tau \cosh \eta_s, \quad x = r \sin \phi, \quad y = r \cos \phi, \quad z = \tau \sinh \eta_s. \quad (3.1)$$

The four velocity is

$$u^\mu = \{u^\tau, u^r, 0, 0\}. \quad (3.2)$$

With  $u^\tau = \sqrt{1 + (u^r)^2}$ . We evolve the relativistic Navier-Stokes equations (2.10), which under these symmetry assumptions become 1+1 PDEs with dependence in the coordinates  $\tau$  and  $r$ , and we choose as our evolving variables  $\{\epsilon, u^r\}$ . Along this section we mostly use frame (2.14), which satisfies the conditions (2.12). For details on the numerical code and convergence tests see Appendix A.

### 3.1 QCD equation of state and transport coefficients

The required input from the microscopic quantum field theory, in our case QCD, for the effective field theory of first-order viscous hydrodynamics is the equation of state and the transport coefficients, the shear and bulk viscosities.

We employ a standard and widely used equation of state obtained by using lattice QCD methods by the 2014 HotQCD collaboration [44] which they parameterize by

$$\frac{p}{T^4}(T) = \frac{1}{2} (1 + \tanh [c_t(\bar{t} - t_0)]) \frac{p_{\text{id}} + a_n/\bar{t} + b_n/\bar{t}^2 + d_n/\bar{t}^4}{1 + a_d/\bar{t} + b_d/\bar{t}^2 + d_d/\bar{t}^4}, \quad (3.3)$$

With  $\bar{t} = T/\hat{T}_c$  and

$\hat{T}_c$	$p_{\text{id}}$	$c_t$	$t_0$	$a_n$	$b_n$	$d_n$	$a_d$	$b_d$	$d_d$
154	$95\pi^2/180$	3.8706	0.9761	-8.7704	3.92	0.3419	-1.26	0.8425	-0.0475

With the temperature assumed to be in MeV. We plot the equation of state (3.3) in Fig. 1 (left).

We use shear and bulk viscosities inspired by the ones obtained by the JETSCAPE collaboration [45], which they parameterize as

$$(\eta/s)(T) = (\eta/s)(\hat{T}_c) + (\eta/s)_{\text{slope}}(T - \hat{T}_c) \left(\frac{T}{\hat{T}_c}\right)^{(\eta/s)_{\text{crv}}}, \quad (3.4a)$$

$$(\zeta/s)(T) = \frac{(\zeta/s)_{\text{max}}}{1 + \left(\frac{T - (\zeta/s)_{\text{peak}}}{(\zeta/s)_{\text{width}}}\right)^2}, \quad (3.4b)$$

With

$\hat{T}_c$	$(\eta/s)(\hat{T}_c)$	$(\eta/s)_{\text{slope}}$	$(\eta/s)_{\text{crv}}$	$(\zeta/s)_{\text{peak}}$	$(\zeta/s)_{\text{max}}$	$(\zeta/s)_{\text{width}}$
0.147	0.104	0.425	-0.738	0.170	0.010	0.057

Where the temperature is expressed in GeV. We plot the shear and bulk viscosities (3.4) in Fig. 1 (right).

We emphasize that these transport coefficients were obtained by fitting to experimental data, rather than from a first principle computation in QCD, and this fit was performed by using MIS-based codes. We use them in this paper because our purpose is to provide a proof of principle that the relativistic Navier-Stokes equations are appropriate to describe experimental data; in the future, once these equations are well established for the description of the experimental data, an interesting exercise will be to use a similar approach to rederive the shear and bulk viscosities using the relativistic Navier-Stokes equations.

In order to implement the equation of state and transport coefficients in our numerical code we express them as a function of energy density, that is,  $p(\epsilon)$ ,  $\eta(\epsilon)$ ,  $\zeta(\epsilon)$ , because we use the energy density,  $\epsilon$ , as our evolution variable.



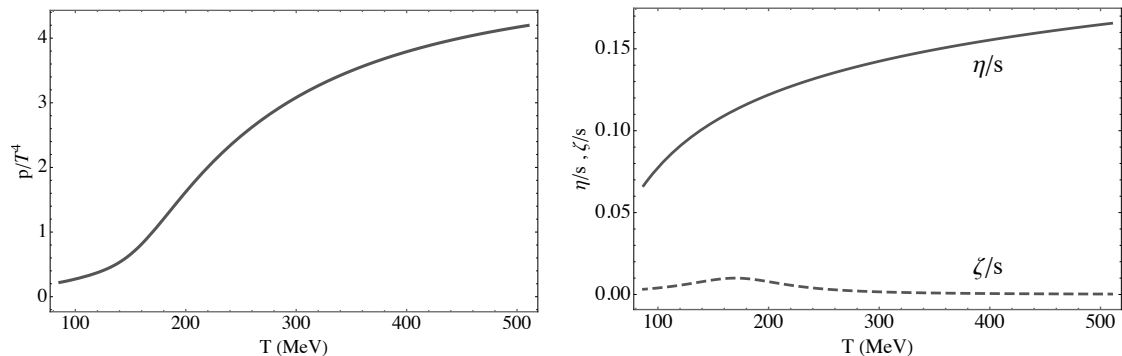


**Figure 1:** Left: QCD equation of state (3.3) from the 2014 HotQCD collaboration [44]. Right: Shear and bulk viscosities (3.4) from JETSCAPE collaboration [45].

### 3.2 Initial data

As initial data we consider a simple geometric setup of the central collision, modelling nuclei as a Woods-Saxon distribution for the energy density, and we integrate the Woods-Saxon profile along the beam axis to obtain the initial energy density distribution. We initialize the evolution at proper time  $\tau_i$ , and we assume vanishing initial transverse velocity. Our initial data is

$$\epsilon|_{\tau_i} = \bar{w} \int_{-\infty}^{\infty} \frac{1}{1 + e^{\frac{\sqrt{r^2 + z^2} - R_0}{a_0}}} dz , \quad (3.5a)$$

$$u_r|_{\tau_i} = 0 , \quad (3.5b)$$

Where  $R_0$  is the characteristic radius of the nucleus,  $a_0$  the width of the skin and  $\bar{w}$  we leave it as a free parameter capturing the initial energy deposited in the fireball, that we find convenient to reexpress as the energy density at the center,  $\epsilon_i := \epsilon|_{\tau_i, r=0}$ . For Pb we use parameters  $R_0 = 6.62$  fm and  $a_0 = 0.546$  fm [46]. For the purposes of this study, we find it sufficient to consider a simple function (3.5a) as our initial data. In the future, we will explore more standard approaches, such as the Glauber model.

The relativistic Navier-Stokes equations (2.10) are of second order in time derivatives, and the initial data includes the first time derivatives of the evolved variables. We propose considering the first time derivatives in the initial data such that they satisfy the ideal equations of motion (2.5), obtaining

$$\partial_\tau \epsilon|_{\tau_i} = - \frac{p(\epsilon|_{\tau_i}) + \epsilon|_{\tau_i}}{\tau_i} , \quad (3.6a)$$

$$\partial_\tau u_r|_{\tau_i} = - \frac{\partial_\epsilon p(\epsilon|_{\tau_i}) \partial_r \epsilon|_{\tau_i}}{p(\epsilon|_{\tau_i}) + \epsilon|_{\tau_i}} . \quad (3.6b)$$

Where the energy and velocities on the right hand side are given by (3.5). The motivation for this choice is as follows. In the absence of a microscopic construction or a specific model to determine the initial time derivatives, if one assumes that the system is described by hydrodynamics, then the system should not be far from satisfying (3.6), with a deviation by first order terms that should be small if the system is in the EFT regime. Other choices like choosing vanishing time derivatives are more in favour of setting the system not so well in the regime of hydrodynamics initially, so maybe this option is not so interesting. A detailed study of evolutions with initial

time derivatives given by the ideal equation of motion, like in (3.6), was performed in [36] for a conformal fluid, for different sets of initial data, indicating that this approach is sensible.

The assumption (3.6) is an interesting approach in the absence of any further motivation, like in the pure geometrical approach considered above. In the case of considering a prehydrodynamics approach in which the time derivatives of the variables can be computed, like, for example, using IP-Glasma [47], then these derivatives can be used in the initial data for the hydrodynamics evolution, replacing the assumption (3.6).

### 3.3 Numerical evolutions

We evolve the relativistic Navier-Stokes equations (2.10) with symmetry assumptions of boost invariance along the beam axis and axial symmetry in the transverse plane, with initial data (3.5) and (3.6), and hydrodynamic frame (2.14). We perform a set of numerical simulations for different values of the initial proper time  $\tau_i$  and initial energy density at the center  $\epsilon_i$ .

As a representative example, in Fig. 2 we show an evolution with initial parameters  $\tau_i=0.6$  fm/c,  $\epsilon_i=100$  GeV/fm<sup>3</sup> (corresponding to temperature  $T = 485$  MeV), in which we plot the temperature as a function of proper time and radius. We stop the evolution at  $\tau=23$  fm/c. We now may construct the freezeout surface, that we define as a constant energy density surface, or, equivalently, a constant temperature surface, by using the equation of state. By choosing a freezeout energy density  $\epsilon_f = 0.05$  GeV/fm<sup>3</sup>, or, equivalently, freezeout temperature  $T_f = 0.12$  GeV, we obtain the black solid line in Fig. 2, that we represent by  $\tau_f(r)$ .

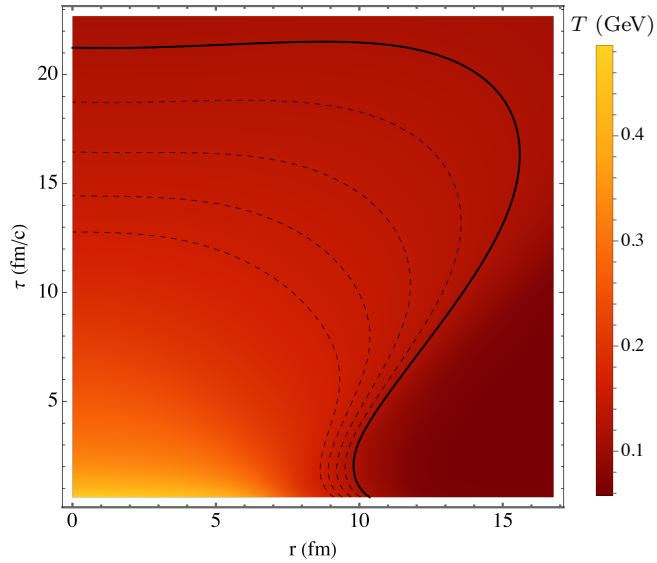


**Figure 2:** Real-time evolution of the temperature in GeV (we evolve energy density and use the equation of state to translate the result to temperature) as a function of proper time  $\tau$  (fm/c) and radius  $r$  (fm), with initial data (3.5) and (3.6) and parameters  $\tau_i = 0.6$  fm,  $\epsilon_i = 100$  GeV/fm<sup>3</sup>. Black solid line indicates freezeout surface at constant temperature  $T_f = 0.12$  GeV. Dashed lines indicate surfaces of constant temperature  $T_f = 0.13, 0.14, 0.15, 0.16$  GeV.

We now obtain the radial velocity of the fluid,  $u_r$ , along the freezeout surface  $\tau_f(r)$ . We plot the profile of the radial velocity  $u_r$  as a function of the radius  $r$  at freezeout in Fig. 3. The information in this plot will be used in the next section to obtain the transverse momentum distribution of hadrons.

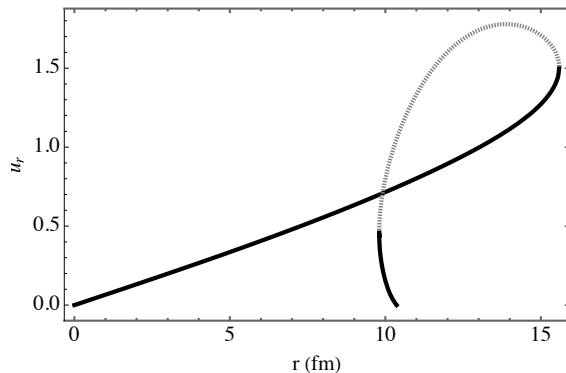


**Figure 3:** From the freezeout surface shown in Fig. 2 we obtain the velocity distribution  $u_r$  at freezeout as a function of  $r$ . The multivaluedness arises from the form of the freezeout surface  $\tau_f(r)$ , that is also multivalued in  $r$ , as can be seen in Fig. 2. The region that we include in the Cooper-Frye expression (3.7) is the black region; the dotted grey region is excluded as it corresponds to particles entering in the surface rather than exiting it.

We verified that this specific solution satisfies good properties of convergence, as described in Appendix A. Moreover, as it is standard in this context, we include a regulator (sometimes called a ‘corona’) in the initial data by adding a very small constant energy density to the initial profile (3.5a). We have verified that the physics does not depend on the value of the regulator, and for this specific simulation we used a value  $\epsilon_{\text{regulator}} = 0.0007 \text{ GeV}/\text{fm}^3$ , which is several orders of magnitude smaller than the value at the center  $\epsilon_i = 100 \text{ GeV}/\text{fm}^3$ .

### 3.4 Description of the experimental data

We consider experimental data from heavy-ion collisions performed at the LHC. In Fig. 4 we show data on the transverse momentum distribution of hadrons (pions, kaons and protons) from Pb–Pb central collisions (0-5% centrality) with centre of mass energy  $\sqrt{s_{NN}} = 2.76 \text{ TeV}$  measured by ALICE [41]. The data is publicly available at <https://www.hepdata.net/record/ins1222333>.

We now use viscous hydrodynamics to provide a description of this data. For the prehydrodynamic region we assume a purely geometric setup as described in Section 3.2. We perform different evolutions with varying initial parameters: initial proper time  $\tau_i$  and initial central energy density  $\epsilon_i$ . For each evolution, we choose a freezeout temperature  $T_f$  and determine the freezeout surface  $\tau_f(r)$  and the corresponding velocity profile  $u_r(r)$ .

We consider a transition from fluid to particles at freezeout surface. For this transition we assume a thermal distribution of hadrons, locally boosted from the local rest frame. This is captured by the Cooper-Frye formula [48], which for an axially symmetric and boost invariant system takes the form [3]

$$\frac{d^2N}{m_\perp dm_\perp dy} \propto \int_0^R r dr \tau_f(r) \left[ m_\perp K_1\left(\frac{m_\perp \sqrt{1+u_r^2}}{T_f}\right) I_0\left(\frac{p_\perp u_r}{T_f}\right) - p_\perp \tau_f'(r) K_0\left(\frac{m_\perp \sqrt{1+u_r^2}}{T_f}\right) I_1\left(\frac{p_\perp u_r}{T_f}\right) \right], \quad (3.7)$$

Which gives the multiplicity density per rapidity  $y$  and transverse mass defined by  $m_\perp := \sqrt{m^2 + p_\perp^2}$ , where  $p_\perp$  is the transverse momentum,  $K_{0,1}$  and  $I_{0,1}$  are modified Bessel functions

and  $R$  is the size of the fireball (i.e., largest value of the radius within the freezeout surface).

For each numerical evolution we use the functions  $\tau_f(r)$  and  $u_r(r)$  in (3.7) to obtain the  $p_\perp$  distribution of pions, kaons and protons. We perform a scan in parameters  $\{\tau_i, \epsilon_i, T_f\}$  and we find that a set that provides a good description of the experimental data is

$$\tau_i = 0.6 \text{ fm}, \quad \epsilon_i = 100 \text{ GeV/fm}^3, \quad T_f = 0.12 \text{ GeV} \quad (3.8)$$

The result of using the Cooper-Frye formula (3.7) for a numerical evolution of the relativistic Navier-Stokes equations with parameters (3.8) is plotted in Fig. 4 in red dashed lines, fitting the three curves with the same parameters, finding good agreement. The numerical evolution corresponding to the values (3.8) is precisely the evolution shown in Fig. 2.

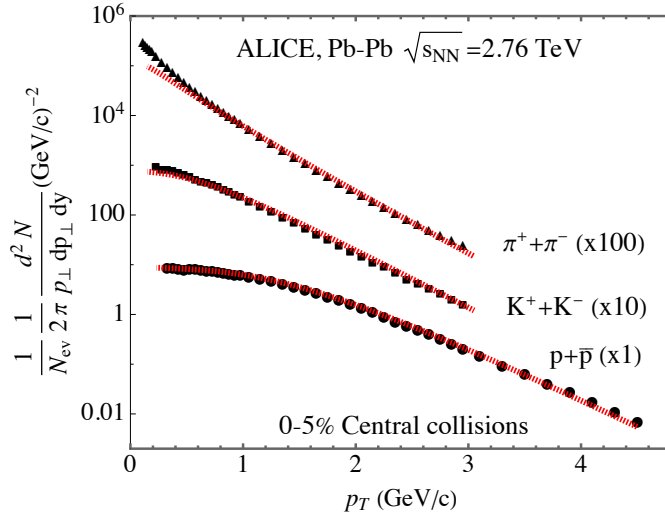


**Figure 4:** Transverse momentum distribution of hadrons measured by ALICE for 0-5% central Pb–Pb collision at  $\sqrt{s_{NN}} = 2.76$  TeV [41]. Dashed red lines correspond to the relativistic Navier-Stokes description using the equation of state (3.3) and transport parameters (3.4), and initial data (3.5) and (3.6) with parameters  $\tau_i = 0.6$  fm/c,  $\epsilon_i = 100$  GeV/fm<sup>3</sup>. The corresponding evolution is presented in Fig. 2, for which we determined the freezeout surface at constant temperature  $T_f = 0.120$  GeV, and obtained the momentum distribution of hadrons by using the Cooper-Frye formula (3.7).

We present a physical interpretation of the plot in Fig. 4, explaining how the radial flow affects the spectra. In situations where there is no significant radial flow, such as in p–p collisions, the Cooper-Frye formula (3.7) reduces to  $\propto m_\perp^{1/2} K_1(m_\perp/T_f)$  and, when plotted versus  $m_\perp$ , the curves have the same shape for all hadrons: this behavior is known as ‘ $m_\perp$  scaling’ [3]. An analogous situation in which the curves are similar for all species occurs at large  $p_\perp$  in Fig. 4. In that case, expression (3.7) gives  $\propto e^{-p_\perp/T_{\text{eff}}}$ , where  $T_{\text{eff}}$  is an effective temperature that captures the blueshift effect of the hydrodynamics expansion of the fluid towards the detector. For low  $p_\perp$ , the curves for the hadrons in Fig. 4 are different for two reasons. First, even in the absence of radial flow, the trivial fact that they are plotted against  $p_\perp$  instead of  $m_\perp$  contributes to this difference. Second, the hydrodynamics expansion of the radial flow generates a flattening of the curves which is more pronounced at low  $p_\perp$  and for heavier particles, which is prominent for kaons and protons; this is one of the most distinctive signatures of the collective behavior of the system. For pions, at low  $p_\perp$  (below  $\sim 0.5$  GeV/c) the pion data presents an excess with respect to the hydrodynamics prediction, and this is due to the contribution of pions from resonance decays, that we are not considering in our description.

We now may wonder how ‘good’ is the fit presented in Fig. 4. One way of evaluating this is the following: we note that the relativistic Navier-Stokes description shown in Fig. 4 is at a similar level of agreement with the experimental data as the results obtained using MIS-based codes. For example, we can compare with results using VISHNU, presented in [49]. It would be interesting to perform more detailed quantitative comparisons with MIS-based results, that we will perform in the future.

We conclude with some comments. First, the normalization constant in (3.7) is put by hand for each species (pions, kaons and protons) separately. This is because chemical freezeout occurs before kinetic freezeout, but this is not captured by our hydrodynamics approach, as our equation of state assumes chemical equilibrium down to kinetic freezeout [3, 50]. Second, when considering the Cooper-Frye formula, in the freezeout surface there can be regions in which the particles are entering the hot region instead of exiting it, and in our case this happens when  $\tau'_f(r) > m_\perp/p_\perp$  [51]. The regions depicted in dotted grey in Fig. 3 satisfy this condition for the relevant range of  $p_\perp$ , and we exclude them from our integral (3.7). Third, when including viscous corrections in the hydrodynamics description the system is not exactly in local thermal equilibrium, and for this reason a correction to the Cooper-Frye formula is usually included [10, 51]; in this work we omit this correction for simplicity. Finally, a standard approach is to include a hadron cascade after freezeout, which captures the subsequent hadron resonance decays, that we do not consider in this work.

### 3.5 Effective field theory analysis

In this section we perform an EFT analysis of our solutions. Evaluating if a solution is in the EFT regime is relevant because if it is not, there is, in principle, no argument to expect that it will provide a good description of QCD, and thus of the QGP.

Given a solution to the hydrodynamics equations, ideal or viscous, it may not be in the EFT regime. We can think of this set of equations as obtained from a truncation of the infinite formal series of the hydrodynamic gradient expansion, and these PDEs admit solutions with arbitrary large gradients. Thus, only a subset of solutions will be in the EFT regime, and for a given solution one has to decide if it is in the EFT regime or not. This decision involves a large degree of arbitrariness: in the formal series of the gradient expansion, where gradients are assumed to be infinitesimal, it is clear which terms are small and negligible with respect to others, but when gradients are finite, as in realistic evolutions used to describe experimental data, this is not defined, and one must provide a specific definition. This definition should be inspired by the formal statement above, keeping the same spirit, and should be physically sensible.

With the purpose of evaluating whether our solution presented in Fig. 2 is in the EFT regime, we measure the different contributions to the stress tensor (2.9). In Fig. 5 we show the ideal and viscous contributions to the  $T^{rr}$  component of the stress tensor: we plot the ideal term,  $|\epsilon u^r u^r + p \Delta^{rr}|$ , in solid black, and the viscous term,  $|- \eta \sigma^{rr} - \zeta \nabla \cdot u \Delta^{rr}|$ , in solid blue, in absolute value, at proper times  $\tau = 0.6, 1.2, 2.8, 6.0$  fm/c, as a function of  $r$ . We now consider a norm over the spatial domain, for example the  $L_1$  norm, and at each time we compute the norm of the viscous terms and the norm of the ideal term and consider their ratio. At the initial time,  $\tau_i = 0.6$  fm/c, the ratio is 32%. Notice that this ratio corresponds to the ratio of the areas under the blue curve and the black curve in the plots in Fig. 5. This ratio quickly decays below 20% at  $\tau = 1.2$  fm/c, 10% at  $\tau = 2.8$  fm/c and 3% at  $\tau = 6.0$  fm/c. We conclude that, as time progresses, the system enters deeper into the EFT regime. The specific point at which the system is considered to have entered the EFT regime depends on the purposes of the analysis and the chosen acceptance threshold; a value of a 32% might be considered marginally in the regime of hydrodynamics.

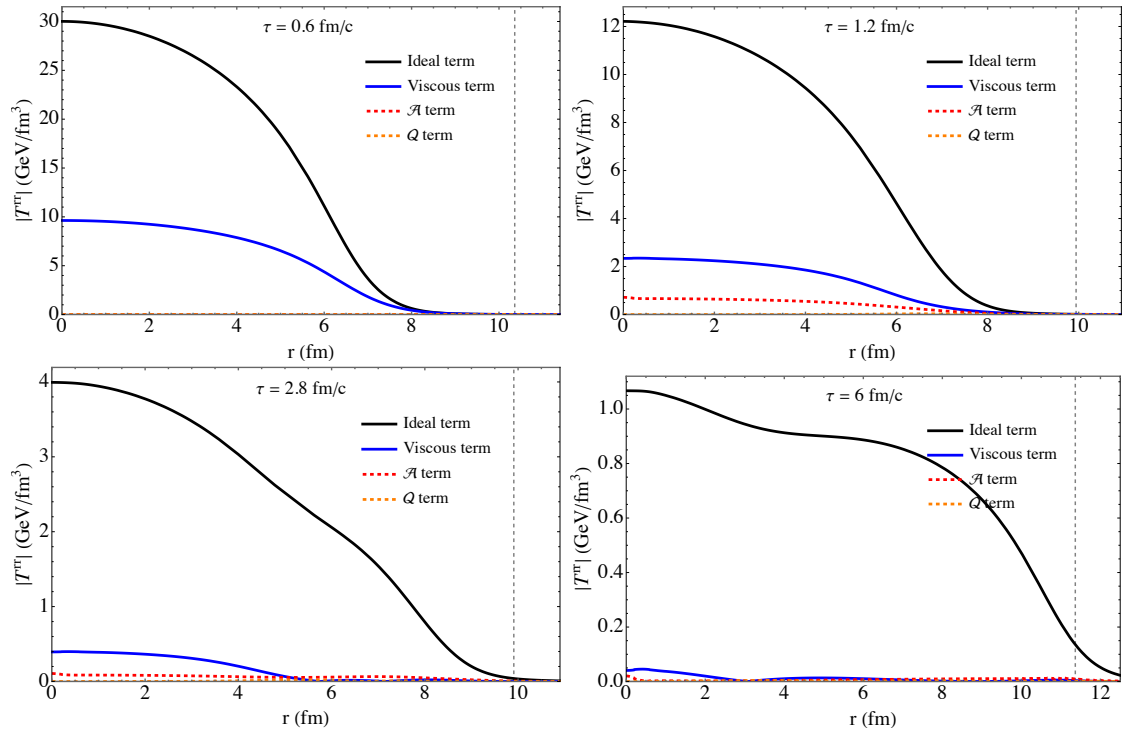


**Figure 5:** We present an EFT analysis of the solution shown in Fig. 2. We display four snapshots at proper times  $\tau = 0.6, 1.2, 2.8, 6.0$  fm/c, in which we plot the different contributions to the  $T^{rr}$  component of the stress tensor as a function of  $r$ : ideal term (solid black), viscous term (solid blue),  $\mathcal{A}$  term (dashed red) and  $\mathcal{Q}^\mu$  term (dashed orange). The vertical dashed line indicates freezeout. At  $\tau = 0.6$  fm/c,  $\mathcal{A}$  and  $\mathcal{Q}^\mu$  terms are vanishing due to the chosen initial conditions. The ratio of the  $L_1$  norms of the viscous and the ideal terms is 32% at  $\tau = 0.6$  fm/c, 20% at  $\tau = 1.2$  fm/c, 10% at  $\tau = 2.8$  fm/c and 3% at  $\tau = 6.0$  fm/c, indicating that the system is entering deeper into the EFT regime as time progresses.

We now present a second argument for why we find it relevant to perform an EFT analysis of our solutions: the physics to first order should be independent of the arbitrarily chosen frame if the system is in the EFT regime, otherwise the equations would lose predictive power. In our case, the field redefinition dependent terms  $\mathcal{A}$  and  $\mathcal{Q}^\mu$  are of second order on-shell, and therefore we should expect them to be much smaller than shear and bulk viscosity terms. In Fig. 5 we include the  $\mathcal{A}$ ,  $\mathcal{Q}^\mu$  contributions to the  $T^{rr}$  component of the stress tensor,  $|\mathcal{A}(u^r u^r + c_s^2 \Delta^{rr})|$ ,  $|2u^r \mathcal{Q}^r|$ , in dashed red and orange respectively. We observe that the  $\mathcal{A}$ ,  $\mathcal{Q}^\mu$  terms are smaller than viscous terms. However, even if locally small, the effect of  $\mathcal{A}$ ,  $\mathcal{Q}^\mu$  terms could potentially accumulate over time giving rise to significant differences, for example due to the non-linear nature of the equations. Alternatively, in a situation in which they are not small, it may potentially happen that performing two evolutions using different frames may still yield similar predictions for the stress tensor.

With this motivation we define the following criterion to assess the effect of using different hydrodynamic frames. We perform two evolutions using two different hydrodynamic frames, and a third evolution using the ideal hydrodynamics equations with similar initial data, and now we compare the difference between the two viscous evolutions and the difference of the

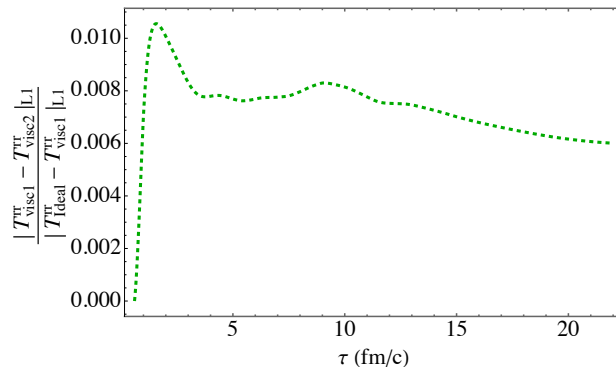


**Figure 6:** We perform two viscous evolutions using different hydrodynamic frames, and a third evolution using ideal hydrodynamics. We then plot the ratio of the  $L_1$  norm of the differences  $T_{rr}^{visc2} - T_{rr}^{visc1}$  and  $T_{rr}^{ideal} - T_{rr}^{visc1}$ , as a function of proper time. We observe that this ratio is of the order of 1%, concluding that the prediction of relativistic Navier-Stokes is robust under changes of frames.

ideal evolution and one of the viscous evolutions. This precisely captures the comparison of the effect of using different frames with the effect of introducing viscosity in the description. For our purposes, at each proper time  $\tau$  we consider the  $L_1$  norm over the spatial domain of the difference of the two viscous evolutions,  $T_{visc1}^{rr} - T_{visc2}^{rr}$ , and the norm of the difference of one of the viscous evolutions and the ideal evolution,  $T_{ideal}^{rr} - T_{visc1}^{rr}$ , for the  $rr$  component of the stress tensor. For the viscous evolution 1 we use frame (2.14) and for the viscous evolution 2 we use a different frame

$$\{a_1, a_2\} = \left\{ \frac{4}{3c_s^2}, \frac{4}{3 - 6c_s^2} \right\}, \quad (3.9)$$

Which also satisfies conditions (2.12). In order to perform a sensible comparison, the two frames must be sufficiently different, if not the solutions will be trivially close to each other; in our case  $a_{1,frame1} = 1.56 a_{1,frame2}$ , so they are significantly different. We plot the ratio of these quantities in Fig. 6. This ratio is of the order of 1%, and, consequently, the effect of using different frames has an impact on the evolution which is about a hundred times smaller than the effect of introducing viscosity in the hydrodynamic description. Thus, we conclude that the relativistic Navier-Stokes equations provide a robust prediction which is independent of the arbitrarily chosen frame even if the system is initially not deep in the EFT regime.

We conclude with some final remarks. First, we observe that the contribution by the bulk viscosity term is small compared to the contribution by the shear term, by evaluating pointwise in spacetime the expressions  $|\eta\sigma^{rr}|$ ,  $|\zeta\nabla \cdot u\Delta^{rr}|$  of the  $rr$  component of the stress tensor. This might be intuitively understood from the relative different values of the viscosities  $\eta/s$  and  $\zeta/s$ , by about a factor of 10, see Fig. 1 (right), and this is reflected in their different contributions to the numerical evolution. Second, we emphasize that in this paper we do not explicitly check frame independence in evolutions using frames of type I, and we leave this for future work. The physics should be also invariant under these change of frames, even if the evolved variables  $\{\epsilon, u_r\}$  will have a different physical meaning; this just corresponds to a different parametrization of the stress tensor which describes the same physics. Finally, let us add that an EFT analysis similar to the one above has been performed in a set of solutions for a conformal fluid in [36].

## 4 Discussion

By using a well-behaved version of the relativistic Navier-Stokes equations, we constructed numerical solutions to describe the QGP created in central heavy-ion collisions, as a proof of principle that these equations are useful for practical applications.

We presented the relativistic Navier-stokes equations for a non-conformal fluid (2.10) in a specific subset of hydrodynamic frames that we find suitable for practical applications. Specifically, we considered field redefinitions (2.7) which are proportional to the lowest-order equations of motion (2.5), that we denoted type II frames. They are suitable because the interpretation of the physical quantities is as in the usual Landau frame, since the novel terms  $\mathcal{A}$ ,  $Q^\mu$  in the constitutive relations of the stress tensor (2.9) are of second or higher order on-shell. Importantly, these terms act as ‘regulators’, in the sense that they ensure that the equations exhibit good properties of well-posedness and causality when conditions (2.12) are satisfied.

The main advantage of relativistic Navier-Stokes with respect to MIS theories is that hydrodynamic frames can be chosen such that for every evolution it is ensured that at every point of spacetime it satisfies good properties of local well-posedness and not faster than light propagation; frame (2.14) provides one such example. In MIS-based codes these conditions of local well-posedness and causality (if known, as they are only known in some specific cases) have to be checked pointwise in spacetime for every evolution, and it is not guaranteed that they will be satisfied; they are actually violated in realistic simulations used to describe the QGP [25–28]. This is the most important argument to state that relativistic Navier-Stokes is a promising alternative to MIS theories, with the advantage being at a fundamental level of well-posedness. A next natural step is to proceed with the actual implementation in a realistic scenario, that we now describe.

We performed real-time evolutions of a boost invariant, axially symmetric fluid with the purpose of modelling the QGP produced in central heavy-ion collisions. We considered a fluid with a QCD equation of state (3.3) and transport parameters (3.4), see Fig. 1. For the initial data we used a Woods-Saxon distribution projected along the beam axis for the energy density and vanishing initial velocities (3.5). For the initial time derivatives, we argued that a suitable choice is to impose that they satisfy the ideal hydrodynamics equations (3.6). We use the hydrodynamic frame (2.14). A representative numerical evolution is shown in Fig. 2; we choose a constant temperature freezeout surface, black solid line. We use the Cooper-Frye formula (3.7) for the transition from fluid to particles. We consider experimental data on the transverse momentum distribution of hadrons from central Pb–Pb collisions at center of mass energy  $\sqrt{s_{NN}} = 2.76$  TeV measured by ALICE at the LHC [41], shown in Fig. 4. In our numerical evolutions we fit the parameters: initial proper time  $\tau_i$ , initial energy density at the center  $\epsilon_i$  and freezeout temperature  $T_f$ , finding that with the values (3.8) we obtain good agreement, as shown in Fig. 4, red dashed lines, providing a good description of the radial flow.

We perform an EFT analysis of our solutions. To determine whether our solution is in the EFT regime, we compare the viscous terms to the ideal terms. Specifically, we consider the  $L_1$  norm of the viscous terms over the spatial domain and a similar norm of the ideal terms, and evaluate their ratio. This ratio is initially 32%, and it decays rapidly over time, indicating that the system is entering into the EFT regime, see Fig. 5. The precise point at which one considers that the system is in the EFT regime will depend on the specific purpose and acceptance threshold. Moreover, by performing numerical evolutions in two different hydrodynamic frames, and a third evolution using ideal hydrodynamics, we verify that the effect of using two different frames is much smaller than the effect of including viscosity in the hydrodynamics description, about 1%, as shown in Fig. 6. We conclude that the prediction of the relativistic Navier-Stokes equations is robust under the change of frames.



There are several natural extensions of the present work. We emphasize that this is a first paper in this direction and we have considered a number of simplifications, focusing on the particularities of the relativistic Navier-Stokes equations. Now that these aspects are more under control, we can proceed with further developments. First, we may extend the dynamics to 2+1 dimensions by relaxing the axial symmetry, which will allow to capture the physics of the elliptic flow. Second, we may consider other prehydrodynamic approaches, such as IP-Glasma [47], which will provide specific initial data for the hydrodynamic evolution. Third, we may incorporate the extra terms in the Cooper-Frye expression that should be considered in the viscous case, that we have omitted for simplicity. Fourth, we may include additional late-stage hadronic physics, like resonance decays. Fifth, we may extend current studies to include baryon density, etc.

Many of these aspects are already included in well developed MIS-based codes, like MUSIC [19–21], SONIC [22] or VISHNU [23], from which they can be imported. A good aim would be to construct similar well developed codes for the relativistic Navier-Stokes equations. Another interesting goal would be to perform a detailed comparison between relativistic Navier-Stokes and MIS theories in realistic descriptions of the experimental data, and explore the specific effects that violations of well-posedness and causality in MIS theories may have on the interpretation of the experimental results.

## Acknowledgments

I thank Jorge Casalderrey-Solana, Pau Figueras, Raimon Luna, David Mateos, Alexandre Serantes and Carlos Vázquez Sierra for very useful discussions. I acknowledge support by the Beatriu de Pinós postdoctoral program under the Ministry of Research and Universities of the Government of Catalonia (2022 BP 00225), by a Maria Zambrano postdoctoral fellowship from the University of Barcelona, by the “Unit of Excellence MdM 2020-2023” award to the Institute of Cosmos Sciences (CEX2019-000918-M) funded by MCIN/AEI/ 10.13039/501100011033/FEDER, UE, and grants PID2019-105614GB-C21, PID2019-105614GB-C22, PID2022-136224NB-C21, PID2022-136224NB-C22 and 2021-SGR-872.

## A Numerical code and convergence test

Our numerical code is implemented in Mathematica. The relativistic Navier-Stokes equations are second order in time, which we reduce to a system of first order time derivatives. For the spatial derivatives we use finite differences of order 6 and for time integration we employ a multi-step Adams-Bashforth method of order 4, with a Courant factor  $dt/dx = 0.1$ . We include Kreiss-Oliger dissipation of order 6 with a coefficient  $\sigma_{KO} = 0.4$ . The polar coordinates used in the transverse plane  $\{r, \phi\}$  introduce a singularity at the origin. We included the singular point  $r = 0$  in the grid, and in the equations of motion we used L’Hôpital’s rule obtaining a non-singular expression. In Fig. 7 we show a convergence test of the solution used to describe the experimental data presented in Fig. 2, finding good properties of convergence. For this test we used resolutions  $N = \{200, 400, 800\}$ . According to our numerical scheme, the expected convergence factor is 4. However, we find slightly lower values, closer to 3, in some regions of the time domain. We suspect that this is possibly an effect of the coordinate singularity at  $r = 0$ .

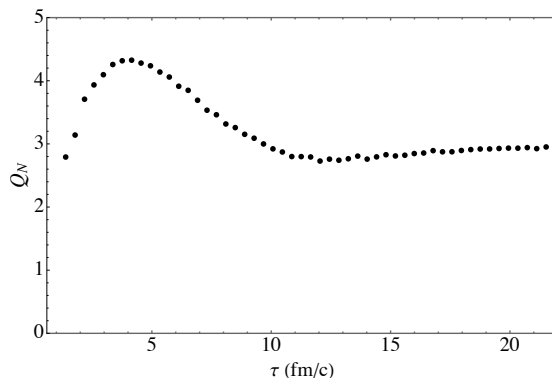


**Figure 7:** Convergence test corresponding to the numerical evolution presented in Fig. 2.

## B Well-posedness for a general stress tensor

The most general stress tensor to first order in the hydrodynamic expansion compatible with Poincare symmetry for a non-conformal fluid can be found in [30] eq. (1). We reproduce it here

$$\begin{aligned}
T^{\mu\nu} = & \left( \epsilon + \chi_1 \frac{\dot{\epsilon}}{\epsilon + p} + \chi_2 \nabla \cdot u \right) u^\mu u^\nu + \left( p + \chi_3 \frac{\dot{\epsilon}}{\epsilon + p} + \chi_4 \nabla \cdot u \right) \Delta^{\mu\nu} \\
& + \lambda u^\mu \left( \dot{u}^\nu + \frac{\partial p}{\partial \epsilon} \frac{\nabla_\perp^\nu \epsilon}{\epsilon + p} \right) + (\mu \leftrightarrow \nu) - \eta \sigma^{\mu\nu},
\end{aligned} \tag{B.1}$$

Where  $\{\chi_{1,2,3,4}, \lambda\}$  are functions of the energy density. The conditions for well-posedness and not faster than light propagation for the stress tensor (B.1) were determined in [30], and we reproduce them here:  $\lambda, \chi_1 \geq 0, \eta \geq 0$

$$\begin{aligned}
9\lambda^2 \chi_2^2 c_s^4 + 6\lambda c_s^2 [\chi_1 (4\eta - 3\chi_4) (2\lambda + \chi_2) + 3\chi_2 \chi_3 (\lambda + \chi_2)] \\
+ [\chi_1 (4\eta - 3\chi_4) + 3\chi_3 (\lambda + \chi_2)]^2 \geq 0,
\end{aligned} \tag{B.2a}$$

$$\lambda \geq \eta, \tag{B.2b}$$

$$c_s^2 (3\chi_4 - 4\eta) \geq 0, \tag{B.2c}$$

$$\lambda \chi_1 + c_s^2 \lambda \left( \chi_4 - \frac{4\eta}{3} \right) \geq c_s^2 \lambda \chi_2 + \lambda \chi_3 + \chi_2 \chi_3 - \chi_1 \left( \chi_4 - \frac{4}{3} \eta \right) \geq 0, \tag{B.2d}$$

$$2\lambda \chi_1 \geq c_s^2 \lambda \chi_2 + \lambda \chi_3 + \chi_2 \chi_3 - \chi_1 \left( \chi_4 - \frac{4}{3} \eta \right). \tag{B.2e}$$

Our specific subset of frames (2.12) satisfies these conditions, and correspond to  $\chi_1 = \chi_2 = a_1(\eta + 3/4\zeta)$ ,  $\chi_3 = a_1 c_s^2(\eta + 3/4\zeta)$ ,  $\chi_4 = a_1 c_s^2(\eta + 3/4\zeta) - \zeta$ ,  $\lambda = a_2(\eta + 3/4\zeta)$ . It is assumed that  $0 \leq c_s^2 \leq 1$ .

Notice that in the most generic stress tensor (B.1) there are 5 parameters  $\{\chi_{1,2,3,4}, \lambda\}$  and in the most generic field redefinition (2.11) there are 3 parameters  $\{\epsilon_{1,2}, \lambda\}$ . There are two parameters that are field redefinition invariant; one of them corresponds to the bulk viscosity. The remaining parameter is obtained by using the ideal equation of motion (2.5a) to replace the bulk viscous tensor  $\nabla \cdot u$  by  $\dot{\epsilon}$  [32], but it is standard to set it to zero.

## References

- [1] P. Romatschke and U. Romatschke, *Relativistic Fluid Dynamics In and Out of Equilibrium*, Cambridge Monographs on Mathematical Physics, Cambridge University Press (5, 2019), [10.1017/9781108651998](https://doi.org/10.1017/9781108651998), [[1712.05815](https://arxiv.org/abs/1712.05815)].
- [2] W. Busza, K. Rajagopal and W. van der Schee, *Heavy Ion Collisions: The Big Picture, and the Big Questions*, *Ann. Rev. Nucl. Part. Sci.* **68** (2018) 339 [[1802.04801](https://arxiv.org/abs/1802.04801)].
- [3] U.W. Heinz, *Concepts of heavy ion physics*, in *2nd CERN-CLAF School of High Energy Physics*, pp. 165–238, 7, 2004 [[hep-ph/0407360](https://arxiv.org/abs/hep-ph/0407360)].
- [4] D.A. Teaney, *Viscous Hydrodynamics and the Quark Gluon Plasma*, in *Quark-gluon plasma 4*, R.C. Hwa and X.-N. Wang, eds., pp. 207–266 (2010), DOI [[0905.2433](https://doi.org/10.1007/978-1-4020-9055-1_10)].
- [5] U. Heinz and B. Schenke, *Hydrodynamic Description of the Quark-Gluon Plasma*, 12, 2024 [[2412.19393](https://arxiv.org/abs/2412.19393)].
- [6] STAR COLLABORATION collaboration, *STAR Experiment Results From Beam Energy Scan Program*, *Phys. Atom. Nucl.* **86** (2023) 758.
- [7] C. Eckart, *The Thermodynamics of irreversible processes. 3.. Relativistic theory of the simple fluid*, *Phys. Rev.* **58** (1940) 919.
- [8] L.D. Landau and E.M. Lifshitz, *Fluid Mechanics*, *Pergamon* (1987) .
- [9] W.A. Hiscock and L. Lindblom, *Generic instabilities in first-order dissipative relativistic fluid theories*, *Phys. Rev. D* **31** (1985) 725.
- [10] D. Teaney, *The Effects of viscosity on spectra, elliptic flow, and HBT radii*, *Phys. Rev. C* **68** (2003) 034913 [[nuc1-th/0301099](https://arxiv.org/abs/nuc1-th/0301099)].
- [11] I. Muller, *Zum Paradoxon der Wärmeleitungstheorie*, *Z. Phys.* **198** (1967) 329.
- [12] W. Israel, *Nonstationary irreversible thermodynamics: A Causal relativistic theory*, *Annals Phys.* **100** (1976) 310.
- [13] W. Israel and J.M. Stewart, *Transient relativistic thermodynamics and kinetic theory*, *Annals Phys.* **118** (1979) 341.
- [14] R. Baier, P. Romatschke, D.T. Son, A.O. Starinets and M.A. Stephanov, *Relativistic viscous hydrodynamics, conformal invariance, and holography*, *JHEP* **04** (2008) 100 [[0712.2451](https://arxiv.org/abs/0712.2451)].
- [15] G.S. Denicol, H. Niemi, E. Molnar and D.H. Rischke, *Derivation of transient relativistic fluid dynamics from the Boltzmann equation*, *Phys. Rev. D* **85** (2012) 114047 [[1202.4551](https://arxiv.org/abs/1202.4551)].
- [16] R.P. Geroch and L. Lindblom, *Dissipative relativistic fluid theories of divergence type*, *Phys. Rev. D* **41** (1990) 1855.
- [17] L. Lehner, O.A. Reula and M.E. Rubio, *Hyperbolic theory of relativistic conformal dissipative fluids*, *Phys. Rev. D* **97** (2018) 024013 [[1710.08033](https://arxiv.org/abs/1710.08033)].
- [18] P. Montes, M.E. Rubio and O.A. Reula, *Numerical simulations of divergence-type theories for conformal dissipative fluids*, [2304.08584](https://arxiv.org/abs/2304.08584).

- [19] B. Schenke, S. Jeon and C. Gale, *(3+1)D hydrodynamic simulation of relativistic heavy-ion collisions*, *Phys. Rev. C* **82** (2010) 014903 [[1004.1408](#)].
- [20] B. Schenke, S. Jeon and C. Gale, *Elliptic and triangular flow in event-by-event (3+1)D viscous hydrodynamics*, *Phys. Rev. Lett.* **106** (2011) 042301 [[1009.3244](#)].
- [21] J.-F. Paquet, C. Shen, G.S. Denicol, M. Luzum, B. Schenke, S. Jeon et al., *Production of photons in relativistic heavy-ion collisions*, *Phys. Rev. C* **93** (2016) 044906 [[1509.06738](#)].
- [22] M. Habich, J.L. Nagle and P. Romatschke, *Particle spectra and HBT radii for simulated central nuclear collisions of C + C, Al + Al, Cu + Cu, Au + Au, and Pb + Pb from  $\sqrt{s} = 62.4 - 2760$  GeV*, *Eur. Phys. J. C* **75** (2015) 15 [[1409.0040](#)].
- [23] C. Shen, Z. Qiu, H. Song, J. Bernhard, S. Bass and U. Heinz, *The iEBE-VISHNU code package for relativistic heavy-ion collisions*, *Comput. Phys. Commun.* **199** (2016) 61 [[1409.8164](#)].
- [24] F.S. Bemfica, M.M. Disconzi, V. Hoang, J. Noronha and M. Radosz, *Nonlinear Constraints on Relativistic Fluids Far from Equilibrium*, *Phys. Rev. Lett.* **126** (2021) 222301 [[2005.11632](#)].
- [25] C. Plumberg, D. Almaalol, T. Dore, J. Noronha and J. Noronha-Hostler, *Causality violations in realistic simulations of heavy-ion collisions*, *Phys. Rev. C* **105** (2022) L061901 [[2103.15889](#)].
- [26] C. Chiu and C. Shen, *Exploring theoretical uncertainties in the hydrodynamic description of relativistic heavy-ion collisions*, *Phys. Rev. C* **103** (2021) 064901 [[2103.09848](#)].
- [27] EXTREME collaboration, *Causality violations in simulations of large and small heavy-ion collisions*, *Phys. Rev. C* **109** (2024) 034908 [[2311.02210](#)].
- [28] T.S. Domingues, R. Krupczak, J. Noronha, T.N. da Silva, J.-F. Paquet and M. Luzum, *The effect of causality constraints on Bayesian analyses of heavy-ion collisions*, [2409.17127](#).
- [29] F.S. Bemfica, M.M. Disconzi and J. Noronha, *Causality and existence of solutions of relativistic viscous fluid dynamics with gravity*, *Phys. Rev. D* **98** (2018) 104064 [[1708.06255](#)].
- [30] F.S. Bemfica, M.M. Disconzi and J. Noronha, *Nonlinear Causality of General First-Order Relativistic Viscous Hydrodynamics*, *Phys. Rev. D* **100** (2019) 104020 [[1907.12695](#)].
- [31] F.S. Bemfica, M.M. Disconzi and J. Noronha, *First-Order General-Relativistic Viscous Fluid Dynamics*, *Phys. Rev. X* **12** (2022) 021044 [[2009.11388](#)].
- [32] P. Kovtun, *First-order relativistic hydrodynamics is stable*, *JHEP* **10** (2019) 034 [[1907.08191](#)].
- [33] M.G. Alford, L. Bovard, M. Hanauske, L. Rezzolla and K. Schwenzer, *Viscous Dissipation and Heat Conduction in Binary Neutron-Star Mergers*, *Phys. Rev. Lett.* **120** (2018) 041101 [[1707.09475](#)].
- [34] M. Chabanov and L. Rezzolla, *Numerical modelling of bulk viscosity in neutron stars*, [2311.13027](#).

- [35] M. Chabanov and L. Rezzolla, *Impact of bulk viscosity on the post-merger gravitational-wave signal from merging neutron stars*, [2307.10464](#).
- [36] Y. Bea and P. Figueras, *Field redefinitions and evolutions in relativistic Navier-Stokes*, [2312.16671](#).
- [37] H. Bantilan, Y. Bea and P. Figueras, *Evolutions in first-order viscous hydrodynamics*, *JHEP* **08** (2022) 298 [[2201.13359](#)].
- [38] A. Pandya and F. Pretorius, *Numerical exploration of first-order relativistic hydrodynamics*, *Phys. Rev. D* **104** (2021) 023015 [[2104.00804](#)].
- [39] A. Pandya, E.R. Most and F. Pretorius, *Conservative finite volume scheme for first-order viscous relativistic hydrodynamics*, [2201.12317](#).
- [40] A. Pandya, E.R. Most and F. Pretorius, *Causal, stable first-order viscous relativistic hydrodynamics with ideal gas microphysics*, *Phys. Rev. D* **106** (2022) 123036 [[2209.09265](#)].
- [41] ALICE collaboration, *Centrality dependence of  $\pi$ ,  $K$ ,  $p$  production in Pb-Pb collisions at  $\sqrt{s_{NN}} = 2.76$  TeV*, *Phys. Rev. C* **88** (2013) 044910 [[1303.0737](#)].
- [42] F.S. Bemfica, M.M. Disconzi and P.J. Graber, *Local well-posedness in Sobolev spaces for first-order barotropic causal relativistic viscous hydrodynamics*, [2009.01621](#).
- [43] H. Freistuhler, *Nonexistence and existence of shock profiles in the Bemfica-Disconzi-Noronha model*, *Phys. Rev. D* **103** (2021) 124045 [[2103.16661](#)].
- [44] HOTQCD collaboration, *Equation of state in (2+1)-flavor QCD*, *Phys. Rev. D* **90** (2014) 094503 [[1407.6387](#)].
- [45] J.E. Parkkila, A. Onnerstad and D.J. Kim, *Bayesian estimation of the specific shear and bulk viscosity of the quark-gluon plasma with additional flow harmonic observables*, *Phys. Rev. C* **104** (2021) 054904 [[2106.05019](#)].
- [46] H. De Vries, C.W. De Jager and C. De Vries, *Nuclear charge and magnetization density distribution parameters from elastic electron scattering*, *Atom. Data Nucl. Data Tabl.* **36** (1987) 495.
- [47] B. Schenke, C. Shen and P. Tribedy, *Features of the IP-Glasma*, *Nucl. Phys. A* **982** (2019) 435 [[1807.05205](#)].
- [48] F. Cooper and G. Frye, *Comment on the Single Particle Distribution in the Hydrodynamic and Statistical Thermodynamic Models of Multiparticle Production*, *Phys. Rev. D* **10** (1974) 186.
- [49] H. Song, S. Bass and U.W. Heinz, *Spectra and elliptic flow for identified hadrons in 2.76A TeV Pb + Pb collisions*, *Phys. Rev. C* **89** (2014) 034919 [[1311.0157](#)].
- [50] U.W. Heinz and P.F. Kolb, *Two RHIC puzzles: Early thermalization and the HBT problem*, in *18th Winter Workshop on Nuclear Dynamics*, 4, 2002 [[hep-ph/0204061](#)].
- [51] S. Jeon and U. Heinz, *Introduction to Hydrodynamics*, *Int. J. Mod. Phys. E* **24** (2015) 1530010 [[1503.03931](#)].